$p+D\rightarrow p+p+n$ Reaction at $6.5\leq E_p\leq 13$ MeV*

A. NIILER,† C. JOSEPH,‡ V. VALKOVIC,§ W. VON WITSCH,|| AND G. C. PHILLIPS
T. W. Bonner Nuclear Laboratories, Rice University, Houston, Texas 77001

(Received 20 November 1968)

The $D(p, 2p)n$ reaction was studied in a kinematically complete experiment at proton bombarding energies of 6.5–13.0 MeV. Silicon surface-barrier detectors were used to record coincident proton-energy spectra at the two sets of angles $\theta_1=30°$, $\theta_2=30°$ and $\theta_1=30°$, $\theta_2=\theta_p$, where θ_1 and θ_2 are on opposite sides of the beam axis and θ_p is the proton angle corresponding to an n-p system with low relative energy recoiling at $\theta_1=30°$. The spectra at $\theta_1=30°$, $\theta_2=30°$ were dominated by the direct knockout or quasifree mechanism and the spectra at $\theta_1=30°$, $\theta_2=\theta_p$ were dominated by the two-step sequential decay mechanism $p+D\rightarrow p+d^*\rightarrow p+p+n$, where d^* is a short-lived particle composed of a neutron and a proton in a $^1S_0$ configuration. The Kuckes-Wilson-Cooper form of the spectator-model calculation gives a good qualitative fit to the knockout data. A least-squares fit of three forms of the density-of-states function to the $E_p=11$ MeV, $\theta_1=30°$, $\theta_p=77°$ data gave the best result with the renormalized density-of-states function. Including the statistically most significant, independently measured spectra at bombarding energies of 9, 11, 12, and 13 MeV, a neutron-proton singlet scattering length of -23.9 ± 0.8 fm is obtained.

1. INTRODUCTION

NUCLEAR reactions which leave three particles in the final state have been studied with increasing interest in recent years, especially in cases where the final state involves strong interactions between pairs of nucleons.[1–11] Enhancements in the cross section can be due to a number of different reaction mechanisms. These are as follows: (1) interaction of two of the final-state particles in a state of their composite system prior to their breakup into two separate particles,[1,2,5,6] (2) quasifree knockout in which the bombarding particle interacts mainly with one of the target constituents, with the remainder of the target behaving as a "spectator" particle,[3,5,12–14] (3) simultaneous breakup of the three particles into the phase space available to them,[1] (4) order of emission interference,[1] (5) rescattering effects,[15–17] and (6) spatial localization.[18] Diagrams representing these mechanisms are shown in Fig. 1. The coherent addition of the amplitudes from each of these effects is possible, but since such interferences have not been observed, they have been neglected in the present paper.

It is of utmost importance to understand the contributions from each of these effects as a function of the kinematic region observed so that experimental separation between the various effects can be accomplished. This separation is usually possible in the kinematically complete experiment. It is usually not possible in the kinematically incomplete experiment, because even in regions where one process should predominate, another process can significantly influence the observed spectra.[19] In the nucleon-on-deuteron reactions, only the first three graphs of Fig. 1 are known to contribute. In order to observe interference effects, states of two pairs of final-state particles must be observable in exactly the same kinematic region. This condition is not generally met for the nucleon-on-deuterium reaction. No spatial localization effects have been observed for this

* Work supported in part by the U.S. Atomic Energy Commission.

† Present address: Los Alamos Scientific Laboratory, Los Alamos, N.M.

‡ Present address: Institut de Physique Nucléaire, Lausanne, Switzerland.

§ Present address: Institut "Ruder Boskovic," Zagreb, Yugoslavia.

|| On leave from Max Planck Institut für Kernphysik, Heidelberg, Germany.

[1] W. D. Simpson, W. R. Jackson, and G. C. Phillips, Nucl. Phys. **A103**, 97 (1967); J. D. Bronson, W. D. Simpson, W. R. Jackson, and G. C. Phillips, *ibid.* **68**, 241 (1965); V. Valkovic, W. R. Jackson, Y. S. Chen, S. T. Emerson, and G. C. Phillips, *ibid.* **A96**, 241 (1967); V. Valkovic, C. Joseph, S. T. Emerson, and G. C. Phillips, *ibid.* **A106**, 138 (1968); S. T. Emerson, Ph.D. thesis, Rice University, 1968 (unpublished); M. C. Taylor, Ph.D. thesis, Rice University, 1968 (unpublished).

[2] P. D. Parker, P. F. Donovan, J. V. Kane, and J. F. Mollenauer, Phys. Rev. Letters **14**, 15 (1965).

[3] I. Slaus, J. W. Verba, J. R. Richardson, R. F. Carlson, and L. S. August, Phys. Letters **23**, 358 (1966).

[4] M. Cerineo, K. Ilakovac, I. Slaus, P. Tomas, and V. Valkovic, Phys. Rev. **133**, B948 (1964).

[5] P. F. Donovan, Rev. Mod. Phys. **37**, 503 (1965).

[6] H. Brückman, W. Kluge, and L. Schänzler, Phys. Letters **24B**, 649 (1967).

[7] B. L. Cohen, E. C. May, and T. M. O'Keefe, Phys. Rev. Letters **18**, 962 (1967).

[8] E. Baumgartner, H. E. Conzett, E. Schields, and R. T. Slobodrian, Phys. Rev. Letters **16**, 105 (1966).

[9] R. T. Slobodrian, J. S. C. McKee, W. F. Tivol, D. T. Clark, and T. A. Tombrello, Phys. Letters **25B**, 19 (1967).

[10] K. W. McVoy, Phys. Rev. **121**, 1401 (1961); M. Bander, *ibid.* **134**, B1052 (1964); R. P. Haddock, R. M. Salter, Jr., M. Zeller, J. B. Czirr, and D. R. Nygren, Phys. Rev. Letters **14**, 318 (1965).

[11] C. Moazed, J. E. Etter, H. D. Holmgren, and M. A. Waggoner, Rev. Mod. Phys. **37**, 441 (1965).

[12] A. Niiler, C. Joseph, V. Valkovic, and G. C. Phillips, Bull. Am. Phys. Soc. **12**, 1174 (1967).

[13] R. J. Griffiths and K. M. Knight, Nucl. Phys. **54**, 56 (1964).

[14] A. F. Kuckes, R. Wilson, and P. F. Cooper, Jr., Ann. Phys. (N.Y.) **15**, 193 (1961).

[15] V. Valkovic, C. Joseph, A. Niiler, and G. C. Phillips, Nucl. Phys. **A116**, 497 (1968).

[16] C. Kacser and I. J. R. Aitchison, Rev. Mod. Phys. **37**, 350 (1965).

[17] J. Lang, R. Müller, W. Wolfli, R. Bosch, and P. Marmier, Nucl. Phys. **88**, 576 (1966); W. Bohne, D. Hilscher, H. Homeyer, H. Morgenstern, and J. A. Schleer, *ibid.* **A106**, 442 (1967).

[18] G. C. Phillips, T. A. Griffy, and L. C. Biedenharn, Nucl. Phys. **21**, 327 (1960).

[19] I. Slaus, Rev. Mod. Phys. **39**, 567 (1967).

TABLE I. Experimental values of n-n scattering lengths.

Reaction	Scattering lengths (fm)	Bombarding energy (MeV)	Reference
$d(\pi^-,\gamma)2n$	$a_{nn}=-16.4\pm1.3$	200	10
$T(d,{}^3\mathrm{He})2n$	$a_{nn}=-16.1\pm1.0$	32.5	8
$d(n,p)2n$	$a_{nn}=-22.5\pm1.0$	14.4	4
$p(p,p)p$	$a_{pp}=-7.817\pm0.007$	low energy	26
${}^3\mathrm{He}(d,T)2p$	$a_{pp}=-7.69^{+0.61}_{-0.67}$	29.8	8
${}^3\mathrm{He}({}^3\mathrm{He},\alpha)2p$	$a_{pp}=-7.7$	43.7, 53	9
$p(n,n)p$	$a_{np}=-23.678\pm0.028$	<1	26
$p(d,2p)n$	$a_{np}=-19.0\pm2.5$	51.5	6
$d(p,2p)n$	$a_{np}=-23.8\pm0.5$	16.0	23
$d(p,2p)n$	$a_{np}=-23.9\pm0.8$	9–13	present work
$d(n,2n)p$	$a_{nn}=-16.4\pm2.9$	14.4	a

[a] B. Zeitnitz, R. Maschow, and P. Suhr, Phys. Letters **28B**, 420 (1969).

reaction. In fact, it would be quite difficult to distinguish this effect from a final-state interaction between the neutron and proton due to the effect of the singlet state, since both are expected to occur at low relative n-p energies.

Since the phase-space effect can be calculated exactly, only the final-state interaction (FSI) and quasifree knockout (QF) processes require thorough experimental investigation. In order to study the relative effects of the FSI and QF processes, kinematic conditions must be chosen such that where one process is most likely, the other one is least likely and vice versa. Thus, the FSI is to be studied in the region where low nucleon-nucleon relative energies are observable while the neutron energy remains as high as possible. On the other hand, the QF process must be studied where the spectator energy approaches zero while the nucleon-nucleon relative energies remain high. Since in the kinematically complete experiment all particle energies and the relative energies of all pairs of particles are uniquely determined, the selection of the proper kinematic conditions is possible. A complete discussion of the kinematics of three-particle final states is given in Ref. 1. The spectra in which strong FSI are observable are fitted with the Phillips-Griffy-Biedenharn (PGB)[18] density-of-states function. Where the spectra show strong QF effects, the fitting is done with the Kuckes-Wilson-Cooper (KWC)[14] form of the spectator-model calculation.

The neutron-neutron singlet scattering length is probably one of the most important datum which is to be extracted only from experiments with three particles in the final state, since free-neutron targets are not yet available. For kinematically incomplete experiments where more than one pair of final-state particles interact strongly, the Watson-Migdal theory[20,21] has been unable to give values for a_{nn} and a_{pp} which are consistent with charge symmetry with sufficient accuracy. The main reason why the results are not very accurate is that the Born and impulse approximations used in many analyses are not valid at the bombarding energies used in these experiments. Also, in most cases, a "secondary" FSI can interfere sufficiently with the "primary" one to cast doubt on the completeness of the analyses. In the two experiments $T(d,{}^3\mathrm{He})2n$ [8] and

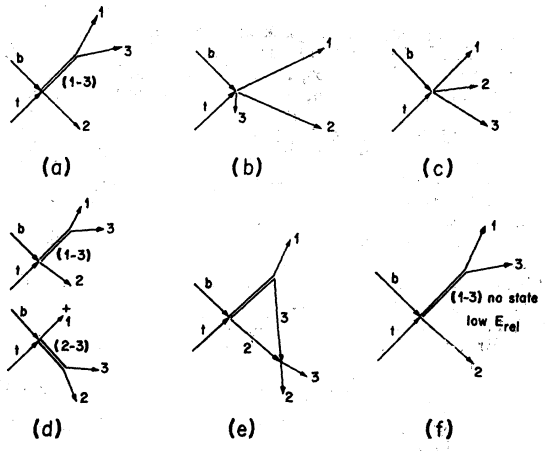

FIG. 1. Diagrams representing the various reaction mechanisms possible in three-body final states: (a) two-step sequential decay, (b) quasifree knockout, (c) simultaneous breakup into phase space, (d) order of emission interference, (e) rescattering, and (f) spatial localization.

[20] K. M. Watson, Phys. Rev. **88**, 1163 (1952).
[21] A. B. Migdal, Zh. Eksperim. i Teor. Fiz. **28**, 3 (1955) [English transl.: Soviet Phys.—JETP **1**, 2 (1955)].

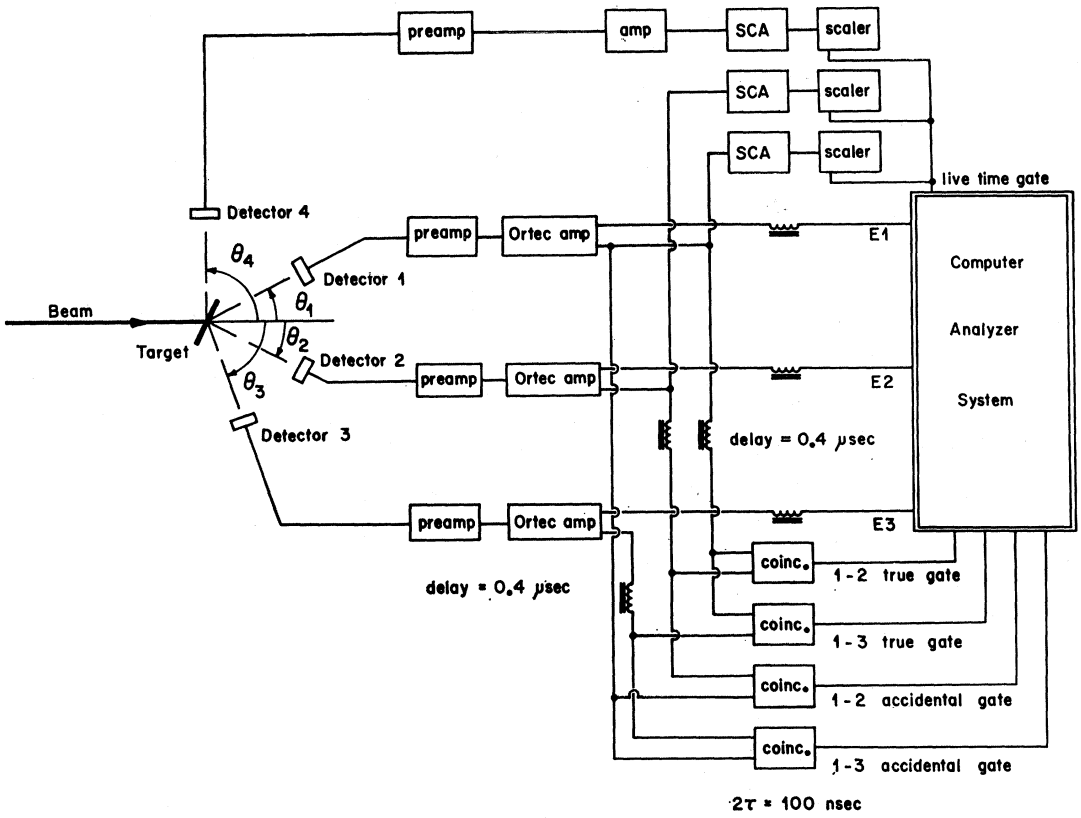

FIG. 2. Block diagram of the expermental layout as used in run 3.

^{3}He(^{3}He, α)$2p$,[9] where the bombarding energies were higher, and no significant contribution from "secondary" final-state interactions was observed, the results were somewhat improved. The $d(\pi^-,\gamma)2n$ reaction,[10] in which there is only one pair of strongly interacting particles in the final state, yields a value for the neutron-neutron scattering length which is probably the most trustworthy to date. Table I gives a partial list of the nucleon-nucleon singlet scattering lengths as obtained by various experiments.

As suggested by van Oers and Slaus,[22] the comparison procedure should be tried in the case of the kinematically complete experiments to extract the a_{nn}. This means a model must be found which yields either of the well-known singlet a_{np} or a_{pp} from reactions where the n-p and p-p final-state interactions are possible. Using this model, one can then have confidence in the a_{nn} extracted from a reaction, where the n-n final-state interaction is produced by the same mechanism. Only recently have efforts at extracting the a_{np} from kinematically complete experiments met with good success.[23,24] In the present work, the a_{np} is obtained from the $D(p,2p)n$ reaction using the PGB density-of-states (DOS) function. A test of FSI theory against the known value of a_{np} is a major purpose of this paper.

2. EXPERIMENT

The data were taken in five separate runs, each of which differed from the others in some experimental detail. The description of the setup for the run during which most of the data were taken is given in full, and the differences made for other runs will be pointed out.

A proton beam from the Rice University tandem Van de Graaff accelerator was used to bombard a deuterated polyethylene foil target of approximately 1.0 mg/cm^2 thickness. Four silicon surface-barrier detectors were mounted in the scattering chamber with three of them in fixed positions and the fourth one continuously movable. Referring to Fig. 2, $\theta_1=30°$, $\theta_2=30°$, $\theta_4=90°$, and $\theta_3=\theta_p$, where θ_p is the proton scattering angle corresponding to an n-p system with 50-keV internal energy recoiling at $\theta_1=30°$. All detectors were placed at a distance of 5.08 cm from the target and all had circular collimating slits of 25-μ-thickness tantalum. The solid angles subtended by detectors 1, 2, and 4 were 0.82×10^{-3} sr and that by detector 3 was 1.72×10^{-3} sr.

Detector-1, -2, and -3, signals were fed into the

[22] W. T. H. van Oers and I. Slaus, Phys. Rev. **160**, 853 (1967).
[23] D. P. Boyd, P. F. Donovan, B. Marsh, and P. Assimakopoulos, Bull. Am. Phys. Soc. **13**, 567 (1968); D. P. Boyd, P. F. Donovan, and J. F. Mollenauer (private communication).
[24] A. Niiler, C. Joseph, and G. C. Phillips, Bull. Am. Phys. Soc. **13**, 568 (1968).

TABLE II. Data for this experiment. Runs 2 and 4 yielded no data for θ_1-θ_2.

	E_p	θ_1-θ_p	θ_1-θ_2
Run 1	11.0	30-77	30-30
	10.0	30-75.4	30-30
	9.0	30-73.2	30-30
	8.0	30-70.2	30-30
Run 2	6.5	30-63.1	—
	7.5	30-68.3	—
	8.0	30-70.2	—
	8.5	30-71.8	—
	9.5	30-74.3	—
	10.0	30-75.4	—
	10.5	30-76.2	—
Run 3	9.0	30-73.2	30-30
	9.5	30-74.3	30-30
	10.0	30-75.4	30-30
	10.25	30-75.8	30-30
	10.50	30-76.2	30-30
	10.75	30-76.6	30-30
	11.0	30-77.0	30-30
	11.25	30-77.4	30-30
	11.5	30-77.7	30-30
Run 4	9.0	30-73.7	—
	11.0	30-77.4	—
	12.0	30-78.7	—
	12.5	30-79.2	—
	13.0	30-79.7	—
Run 5	11.0	40-40	

analog-to-digital converters (ADC's) of the IBM 1800 computer-analyzer system. True and accidental gating signals were obtained for detector pairs 1-2 and 1-3 by means of a cosmic multiple coincidence unit requiring both fast and slow coincidence. Accidental gating signals were obtained by delaying the detector-1 signal into the fast coincidence unit by 400 nsec more than was required to obtain true coincidences. The coincidence time resolution for all four coincidence conditions was approximately 100 nsec as determined from a delay curve with protons elastically scattered from deuterium in one detector and the recoil deuterons in the other.

A true two-dimensional energy event between detectors 1-2 and 1-3 is written in a buffer area of the computer core upon arrival of a true 1-2 or 1-3 gate signal, whereas an accidental event of the same type is recorded upon arrival of an accidental 1-2 or 1-3 gate. Each word written is tagged with the proper gate and ADC information. After the buffer is filled with 312 words, it is dumped onto magnetic tape while a second buffer is being filled with incoming data. Since the coincident counting rates were in the order of a few per second, computer dead-time errors were negligible.

The polyethylene targets are quite unstable under beam bombardment so that beam integration is not a meaningful monitor of the experiment since the deuterium content of the target varies. Detectors 1 and 2, being at fixed angles of 30°, 30° in the chamber, were used to count the recoil deuterons from the $D(p, p)d$ process and detector 4, at 90°, was used to count the scattered protons. The scalars used to count these elastic scattering events were gated by computer live time; the two-dimensional spectra were then normalized to the elastic p-d data obtained by Wilson[25] with the Rice precision gas scattering chamber.

As was pointed out above, the data in this experiment were gathered in five separate runs. In the first run, since the IBM-1401 computer analyzer was used, data for only one set of angles could be collected at one time. In this case, the data were taken in three-parameter format with a time-to-amplitude converter (TAC) signal corresponding to the time difference between the two detector signals being recorded along with the two energy signals. The time spectrum has a peak approxi-

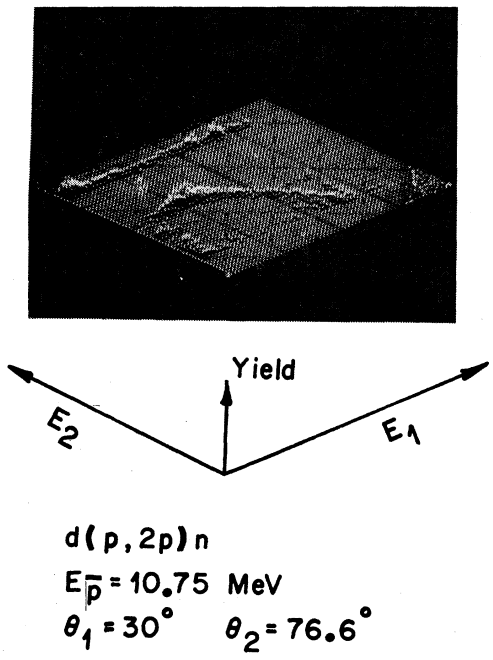

FIG. 3. Photograph of the computer oscilloscope display for a typical run. Population along the curved band is due to the $d(p, 2p)n$ reaction. The straight lines are due to accidental from p-d elastic and p-^{12}C inelastic processes.

[25] A. S. Wilson (private communication).

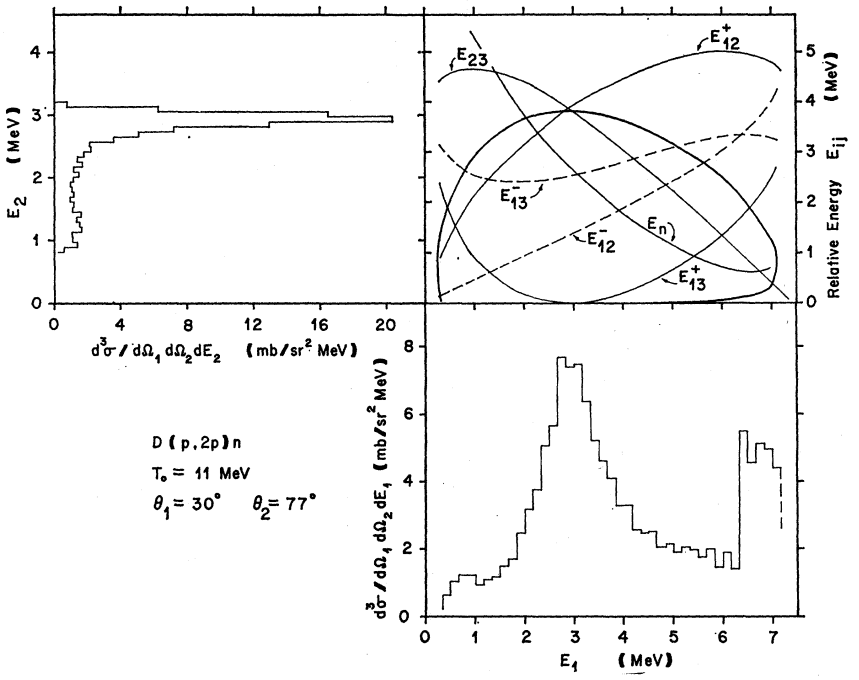

FIG. 4. The kinematics and projected data for $E_p=11$ MeV, $\theta_1=30°$, $\theta_2=77°$. The diagram in the upper right-hand corner depicts the kinematics of this energy angle combination. The heavy solid curve is the locus of kinematically allowed E_1 versus E_2; the lighter lines and dotted lines show the relative energies of the three pairs of final-state particles as a function of E_1. The energy of the undetected neutron as a function of E_1 is indicated by the line marked E_n. To the bottom and left are shown the projections on the E_1 and E_2 axes of the events along the $D(p, 2p)n$ locus with the background subtracted. The ordinate in mb/sr² MeV should be multiplied by 0.866.

mately 15 nsec wide corresponding to true $d(p, 2p)n$ events and a uniform background of accidental events. An off-line computer sort of all three-parameter events was made. An event was tagged as true if its time fell in the true-time window and as accidental if its time fell in a window of the same width but in the uniform, accidental region of the time spectrum. Another run was the first data run with the IBM-1800 computer analyzer and only the $\theta_1=30°$, $\theta_2=\theta_p$ data were obtained with the trues and accidentals collected on separate gates.

The fourth run was made collecting data in the three-parameter E_1-E_2—TAC configuration with the IBM 1800 computer. In this run the detector slits were rectangular rather than circular, and θ_p was the proton scattering angle corresponding to the n-p system with zero relative energy recoiling at 30°. One other spectrum

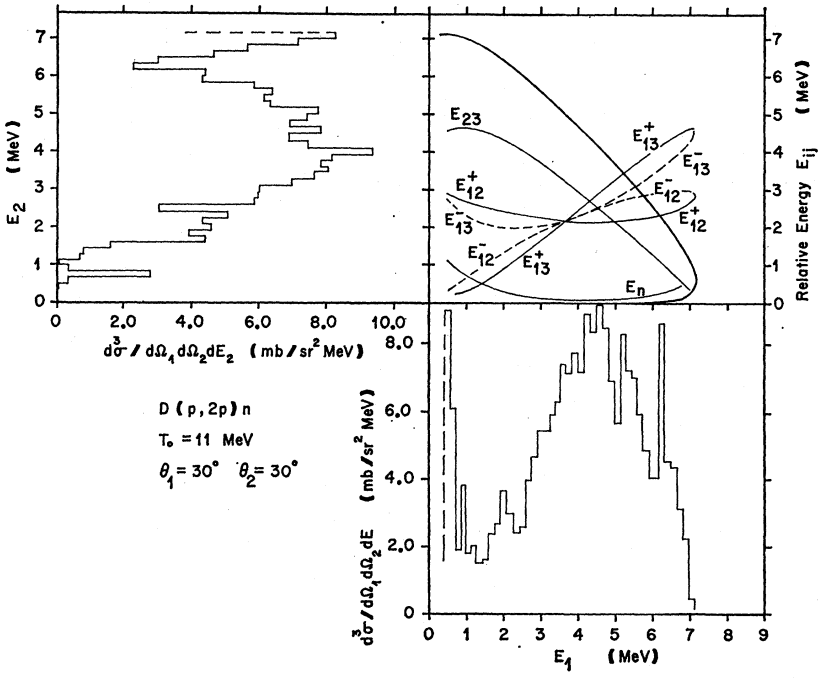

FIG. 5. Some as Fig. 4 for $E_p=11$ MeV, $\theta_1=30°$, $\theta_2=30°$. The one-channel-wide peak at ~6.5 MeV is attributable to imperfect subtraction of the $^{12}C(p, p')$ background. The ordinate in mb/sr² MeV should be multiplied by 0.866.

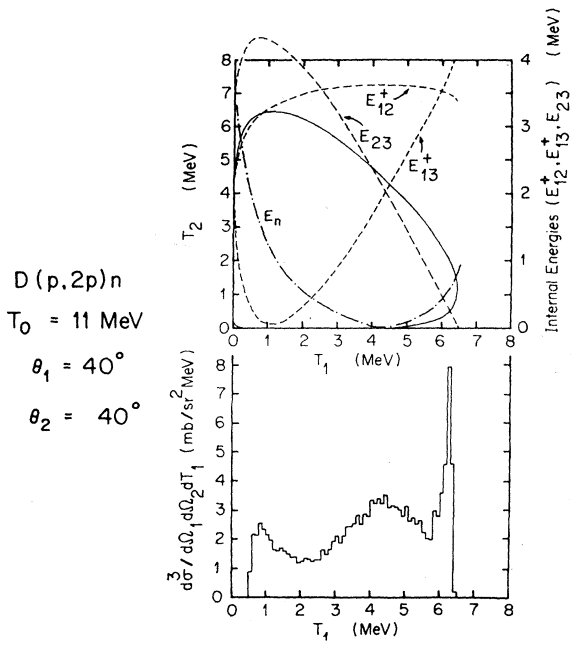

FIG. 6. The ordinate in mb/sr² MeV should be multiplied by 0.866. Same as Fig. 4 for $E_p=11$ MeV, $\theta_1=40°$, $\theta_2=40°$.

was taken at $E_p=11$ MeV, $\theta_1=\theta_2=40°$. The angles were such that both the FSI and QF effects were observable but neither at its optimum. This spectrum was taken in the same format as those in run No. 1 on the IBM-1401 computer.

Table II shows the bombarding energies and angle settings at which data were taken for each run.

3. DATA AND ANALYSIS

Since the kinematics of final states containing three particles have been thoroughly discussed in previous work,[1] only a short summary is necessary here. The coincident measurement of the energies of two of the three final-state particles along with their angles of emission specifies six out of the total of nine kinematic variables involved. Four variables are specified by energy and momentum conservation equations so that the experiment is actually kinematically overdetermined, a fact which allows a convenient background separation. Since the kinematics are completely determined, one can obtain functional relationships between the energy of either of the detected particles and the energy of either of the other two particles, or the relative energies of any of the pairs of final-state particles.

A locus of kinematically allowed energies in the $E1$-$E2$ plane is thus specified for each bombarding energy, reaction Q value, and detector angle combination, where $E1$ and $E2$ are the detected particle energies. For each position along the locus, there exists a unique relative energy for each of the three pairs of particles and an energy for the third undetected particle.

Thus, in the $D(p, 2p)n$ reaction, when the two protons are detected, besides accidental events, the $E1$-$E2$ plane should be populated only along one kinematic locus. An example of the behavior of the actual data is shown in Fig. 3. This figure is a photograph of the computer oscilloscope screen with the data in an isometric plot, the axes being $E1$ and $E2$, and the number of events per energy cell appearing raised above the $E1$-$E2$ plane. A high density of counts can be observed along straight lines corresponding to accidental events due to elastic scattering from deuterium and inelastic scattering from carbon (^{12}C), and also along a curved band corresponding to the $D(p, 2p)n$ reaction.

In Fig. 4, the kinematic situation for the $E_p=11$ MeV, $\theta_1=30°$, $\theta_2=77°$ spectrum is pictured. The solid closed curve in the upper right hand corner depicts the locus of kinematically allowed events in the $E1$-$E2$ plane. The various lighter lines and dotted lines represent the relative energies of the three different pairs of final-state particles as a function of $E1$. Since $E2$ is a quadratic function of $E1$, there are two solutions for the relative energies corresponding to each value of $E1$. $E_{ij}^{\pm}$ are these two solutions and correspond to the two branches of the locus. The energy of the undetected neutron is also shown by the curve labeled E_n.

To the bottom and left side of the kinematics curves, the data along the $D(p, 2p)n$ locus are shown projected on the two energy axes. A peak in the distribution occurs at that value of $E1$-$E2$ which corresponds to a low value of the relative energy between the neutron and the proton detected at $\theta_1=30°$, E_{13}^{+}. In the $E1$ projection of the data, a rise in the yield is also observed for that value of $E1$ which corresponds to a relative energy between the neutron and proton detected at $\theta_2=77°$ (E_{23}) approaching 50 keV. It can be shown that the phase-space effect can also be responsible for a peak in this region of $E1$. Unfortunately, it is not possible to distinguish between these two effects by experimental means in this region of phase space.

Figure 5 shows the kinematic situation and the projected data for the bombarding energy $E_p=11$ MeV and the detector angles $\theta_1=30°$, $\theta_2=30°$. The most striking feature in this spectrum is that the peak in the yield occurs at that $E1$ which corresponds to a minimum in the energy of the undetected neutron. No structure attributable to the two-step sequential decay is observed.

Figure 6 shows the kinematic situation and the projected data for the bombarding energy $E_p=11$ MeV and $\theta_1=\theta_2=40°$. Three distinct peaks are observed in the $E1$ projection of the $E1$-$E2$ spectrum. The central, broad distribution corresponds to the minimum value of the spectator neutron energy. The two outside peaks occur at that $E1$ corresponding to low values of the n-p relative energies, E_{13}^{+} and E_{23}. A comparison of Figs. 4–6 shows the importance of choosing the proper kinematic region in order to separate the FSI and QF effects.

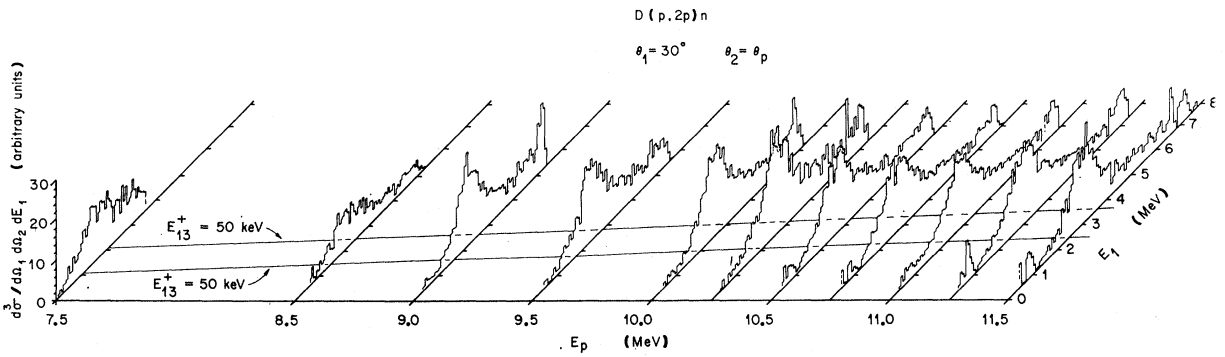

FIG. 7. An isometric plot of the $\theta_1=30°$, $\theta_2=\theta_p$ data projected on the E_1 axis for the energy range 7.5–11.5 MeV. The locus corresponding to 50-keV relative energy between the neutron and the proton detected at 30° in the E_p versus E_1 plane is shown by the lines labeled $E_{13}{}^{+}=50$ keV.

Figure 7 is an isometric plot of the $\theta_1=30°$, $\theta_2=\theta_p$ data projected on the $E1$ axis for the energy range 7.5–11.5 MeV. The principal feature to note is that a peak is observed in the cross section that is always associated with low relative energies between the unobserved neutron and the proton that was detected at 30°. The second proton in each of these cases is detected at the proton scattering angle corresponding to a d^* with 50 keV of internal energy recoiling at 30°. The small, sharp peaks appearing at some bombarding energies around $E1\cong 1$ MeV and $E1\cong 6$–7 MeV are due to imperfect background subtraction since the ADC's used for true and accidental spectra did not have exactly the same gains. Each of these peaks is associated with either inelastic scattering from ^{12}C or p-d elastic scattering.

Figure 8 is the isometric plot of the $\theta_1=30°$, $\theta_2=30°$ data projected on the $E1$ axis over the energy range of 9–11.5 MeV. The line labeled E_n(min) indicates the position of the minimum "spectator" neutron energy, and it can be seen that the center of the broad peak falls quite closely at this minimum neutron energy position for all bombarding energies.

The differential cross section is obtained by use of the relation

$$\frac{d^3\sigma}{d\Omega_1 d\Omega_2 dE_i}=\frac{N_{12}}{N_{e1}}\left(\frac{d\sigma}{d\Omega}\right)_{e1}\frac{1}{\Delta\Omega_2\Delta E_i}, \qquad (1)$$

where N_{12} is the number of coincident events per energy interval, ΔE_i is the energy interval along the E_i axis, $\Delta\Omega_2$ is the laboratory solid angle of detector 2, N_{e1} is the number of recoil deuterons counted in detector 1, and $(d\sigma/d\Omega)_{e1}$ is the recoil deuteron cross section in detector 1 from Ref. 25. The beam intensity, target thickness, and solid angle of the detector counting the recoil deuterons do not enter into the expression for the cross section. Consequently, no accurate measurements of beam intensity nor target thickness need be made, eliminating a large potential source of error.

4. DISCUSSION

A. Reaction Mechanisms

The isometric plots of Figs. 7 and 8 provide a convenient method of identifying the observed structure in the spectra. The peaks in Fig. 7 track along a relative energy $E_{13}{}^{+}\simeq 0$ but not along any other relative energy line or the minimum neutron energy line (these latter

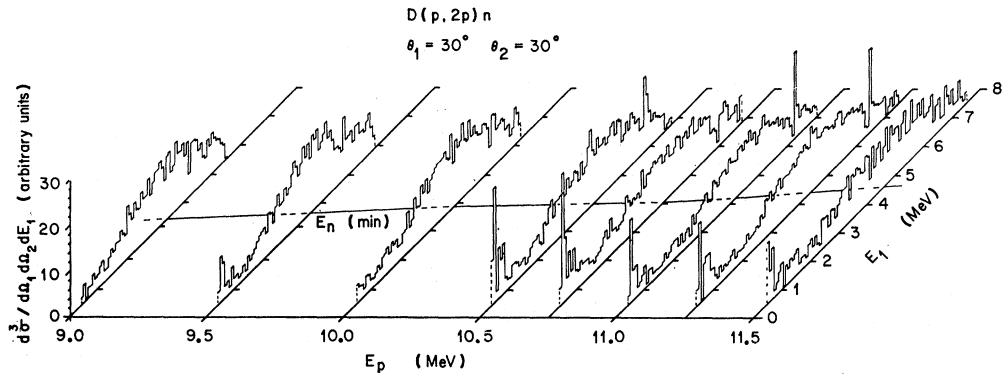

FIG. 8. Isometric plot of the $\theta_1=30°$, $\theta_2=30°$ data projected on the E_1 axis for the energy range 9.0–11.5 MeV. The line labeled E_n gives the position of the minimum neutron energy in the E_p versus E_1 plane.

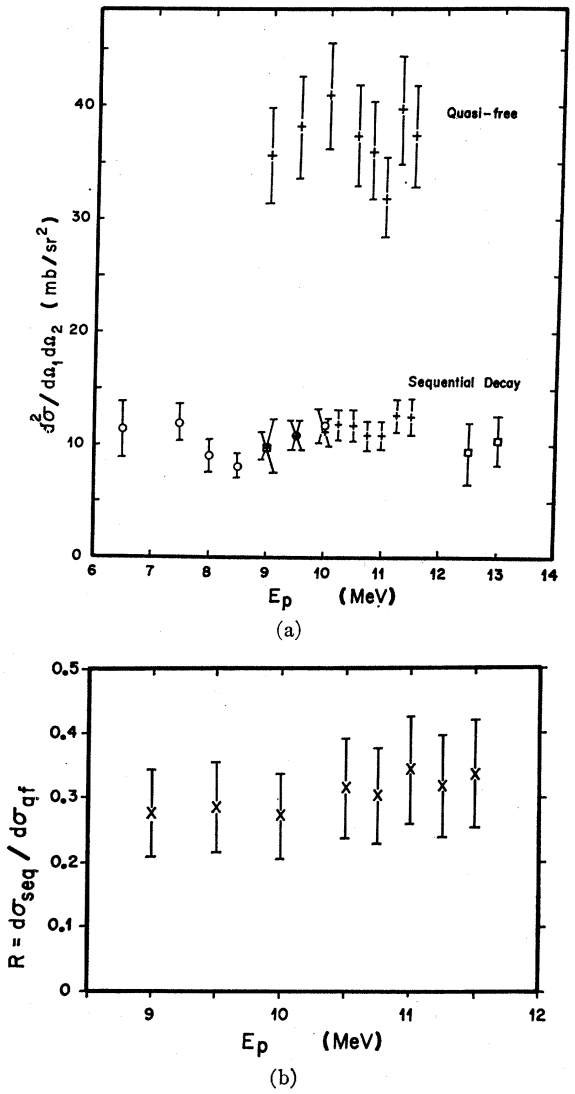

FIG. 9. (a) Cross section for the sequential decay process at $\theta_1=30°$, $\theta_2=\theta_p$ and the QF process at $\theta_1=30°$, $\theta_2=30°$ as a function of the proton bombarding energy. (b) The ratio of $(d^2\sigma/d\Omega_1 d\Omega_2)_{seq}$ to $(d^2\sigma/d\Omega_1 d\Omega_2)_{QF}$ for the energy range 9.0–11.5 MeV. The ordinate in mb/sr^2 MeV should be multiplied by 0.866.

lines are omitted in the figure for clarity). Thus the peaks must be attributed to a final-state interaction between the neutron and the proton detected at 30°. The only known n-p state having effect at this n-p relative energy is the virtual singlet state of the deuteron. By doing angular correlation measurements, Simpson[1] also has shown that the peak tracks only along the $E_{13}{}^{+}\simeq 0$ line. Furthermore, he observed that the maximum in the yield occurs at that set of angles where θ_2 is the proton scattering angle corresponding to an n-p system with $E_{rel}<50$ keV recoiling at θ_1, the set which was used in this experiment.

Similarly, Fig. 8 shows that the broad distribution tracks only along the line corresponding to a minimum neutron energy. Again, other relative energy lines have been omitted for clarity. Thus, this broad peak can be attributed to a process which leaves the neutron with a low laboratory energy. This process is known variously as quasifree scattering or the spectator effect. The study of this process at higher bombarding energies[14] has shown that the maximum yield occurs at the set of angles corresponding to the quasifree recoil axis. This quasifree recoil axis is defined by the angles of a proton proton scattering process having a -2.2247-MeV Q value. For the energies in the present experiment, the quasifree recoil axis varies between $\theta_1=30°$, $\theta_2=45°$ and $\theta_1=30°$, $\theta_2=50°$. Because of the experimental situation, however, it was more convenient to measure this effect at the constant angle settings of 30°-30° over the whole energy range. As a result, since the maximum differential cross section is measured for the sequential process but less than the maximum is measured for the quasifree process, a direct comparison of the two mechanisms is somewhat restricted.

In Fig. 9(a) are shown the measured differential

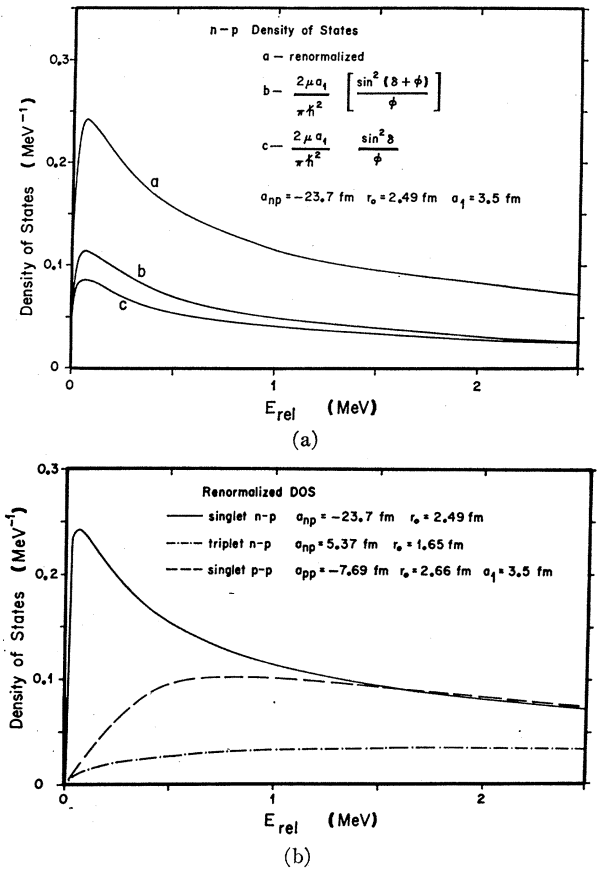

FIG. 10. (a) Three forms of the PGB DOS for the n-p singlet interaction given by Eqs. (2), (3), and (4). (b) The renormalized form of the PGB DOS [Eq. (2)] for the singlet n-p, triplet n-p, and singlet p-p interactions.

cross sections over the energy range 6.5–11.5 MeV for the sequential process and 9–11.5 MeV for the quasifree process. The yield for the sequential decay process represents a summation of those individual channels corresponding to an n-p relative energy $E_{13}^{+}\leq 300$ keV. This 300-keV limit is rather arbitrary in the sense that the $^1S_0$ n-p interaction certainly extends above this value. However, as can be seen from Fig. 4, for example, on the low $E1$ side of the peak where the 1-2 and 2-3 interactions are less important, the yield drops to $\sim 10\%$ of the peak value at the $E_{13}^{+}=300$-keV level. As will be shown later, the noncoherent contributions from the singlet p-p (E_{12}^{+}) and the other singlet n-p (E_{23}) interactions are less than 5% of the yield from the primary singlet n-p (E_{13}^{+}) interaction in this region of the spectrum. The triplet n-p contribution is expected to be smaller still (see Sec. 4 A 1 and Fig. 10). Furthermore, from Fig. 4, it can be seen that the spectator neutron energy is considerably higher than 1 MeV when $E_{13}^{+}<300$ keV so that contributions from the quasifree process in this region should also be negligible.

For the 30°-30° spectra, the yields for the quasifree process represent a summation of yields from individual channels corresponding to $E_n\leq 0.75$ MeV, where E_n is the energy of the undetected neutron. Again, the contribution to the yield from the singlet- and triplet-final-state interactions should be somewhat less than 5% of the quasifree yield in this region of the phase space.

Figure 9(b) shows the ratio $\sigma_{\mathrm{seq}}/\sigma_{\mathrm{qf}}$ from 9.0–11.5 MeV. It is noteworthy that the quasifree process is much stronger than the sequential process in this energy range even though the sequential yield is maximized while the quasifree is not. There is a slight upward trend in this curve, which probably reflects the fact that the quasifree data were not collected on the quasifree recoil axis.

1. Sequential decay. The PGB DOS function was used to fit the spectra at those angles where the spectator neutron energy did not fall below 1.0 MeV. The three forms of the DOS functions which were tried are

$$\rho(k,a_1)=(\mu/\pi h^2k)[(d/dk)(\delta+\phi)-(1/2k)\sin 2(\delta+\phi)], \tag{2}$$

$$\rho(k,a_1)=(2\mu a_1/\pi h^2)[\sin^2(\delta+\phi)/P], \tag{3}$$

$$\rho(k,a_1)=(2\mu a_1/\pi h^2)(\sin^2\delta/P), \tag{4}$$

where $\phi=ka_1$ is the hard-sphere phase shift, a_1 is the interaction radius between two nucleons, δ is the nucleon-nucleon phase shift obtained from the effective range theory, and P is the penetrability, which asymptotically becomes ka_1 for the n-p case. Equations (2)–(4) show the DOS functions as simplified for the n-p case. The more general forms of these expressions can be obtained from Ref. 18. Since only two-body forces are involved, the process must be a two-step sequential decay mechanism in which the first step is the formation of a singlet or triplet two-nucleon state along with the third nucleon, and the second step is the decay of the two-nucleon state. The particles in the two-nucleon state must be localized within the interaction radius a_1 of each other long enough to allow the third nucleon to escape. Since only the phase shifts enter, the calculation is equally applicable both to discrete bound states or to the scattering states. Equation (2) gives the form of the renormalized DOS in which the final-state two-body wave function is normalized inside a large box of radius R. In the case that the final-state wave function is independent of energy for $r\leq a_1$, the expression in Eq. (2) reduces to that in Eq. (3). The Watson form of the DOS is given by Eq. (4).

These three forms of the DOS are shown in Fig. 10(a) for the n-p singlet interaction. It can be seen that there are only small differences among them in terms of the position of the peak and its width. Figure 10(b) shows the renormalized forms of the singlet n-p, the triplet n-p, and the singlet p-p DOS. All curves in Fig. 10 are drawn to scale. The fact that the triplet n-p DOS is more than an order of magnitude smaller than the singlet n-p DOS for $E_{\mathrm{rel}}<300$ keV allows it to be neglected in the calculations.

The cross section for the sequential decay process is given by

$$\sigma_{\mathrm{seq}}(k)=|M_{IF}|^2\rho(k,a_1)\mathfrak{J}(k), \tag{5}$$

where M_{IF} is the matrix element describing the first vertex of the reaction (cf. Fig. 1), $\rho(k,a_1)$ is the DOS function, and $\mathfrak{J}(k)$ is the kinematic factor transforming the detector solid angles from the n-p cm system to the laboratory. The M_{IF} is assumed to have no momentum dependence in all calculations.

A complete expression for the cross section would include, in the first order, a sum of terms like Eq. (5) for each final-state pair of particles in both the singlet and triplet states, a quasifree term and a simultaneous three-body breakup (phase-space) term. Also interference terms should be included in this set. However, in the regions of phase-space where $E_n>1$ MeV and $E_{13}^{+}<300$ keV, all but the singlet 1-3, 1-2, and 2-3 interactions and phase space are neglected. Thus, the cross section becomes

$$\sigma(k)=C_{13}\rho_{13}(k)\mathfrak{J}_{13}(k)+C_{12}\rho_{12}(k)\mathfrak{J}_{12}(k)+C_{23}'\rho_{23}(k)\mathfrak{J}_{23}(k)+C_{\mathrm{ps}}P(k), \tag{6}$$

where $P(k)$ is the differential phase space. Now, over the range of k in the data, $\rho_{23}(k)$ is very nearly a constant, and $\mathfrak{J}_{23}(k)\cong P(k)$ so that the last two terms may be combined:

$$C_{23}'\rho_{23}(k)\mathfrak{J}_{23}(k)+C_{\mathrm{ps}}P(k)\cong(C_{23}'+C_{\mathrm{ps}}')\rho_{23}(k)\mathfrak{J}_{23}(k)=C_{23}\rho_{23}(k)\mathfrak{J}_{23}(k) \tag{7}$$

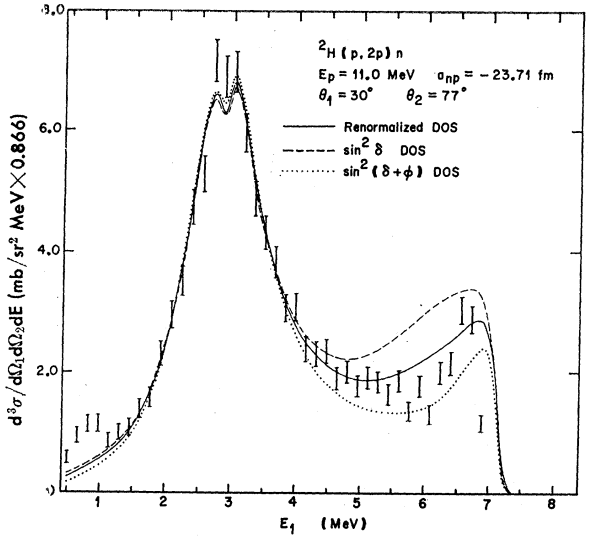

FIG. 11. Fits to the $E_p=11$ MeV, $\theta_1=30°$, $\theta_2=77°$ data with the three forms of the DOS in Eqs. (2), (3), and (4). In all three, $C_{13}=C_{12}=C_{23}=1.0$, $a_{np}=-23.71$ fm, $a_{pp}=7.69$ fm, $r_{0\,np}=2.5$ fm, and $r_{0\,pp}=2.81$ fm. Energy losses in the target are not folded in.

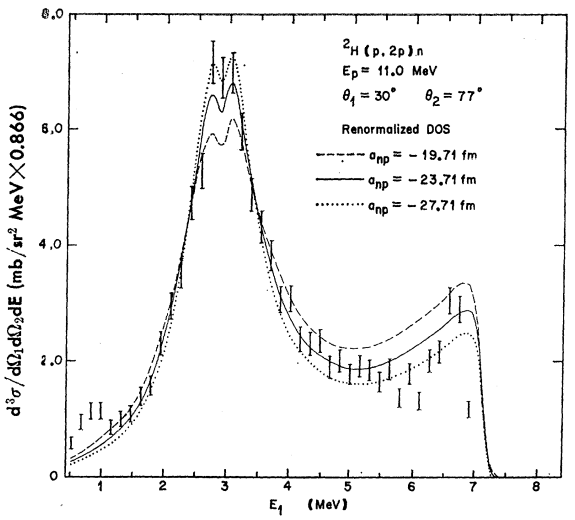

FIG. 13. Fits to the 11 MeV, $\theta_1=30°$, $\theta_2=77°$ data with the renormalized DOS function for the three values of a_{np}, −19.71, −23.71, and −27.71 fm. $C_{13}=C_{12}=C_{23}=1.0$, $a_{pp}=7.69$ fm, $r_{0\,pp}=2.81$ fm, and $r_{0\,np}=2.5$ fm. Energy losses in the target are not folded in.

and

$$\sigma_{\rm seq}(k)=C_{13}\rho_{13}(k)\mathfrak{I}_{13}(k)+C_{12}\rho_{12}(k)\mathfrak{I}_{12}(k)+C_{23}\rho_{23}(k)\mathfrak{I}_{23}(k). \quad (8)$$

Because of the experimental energy thresholds, only the positive (higher-energy) branch of the locus of Fig. 4 is observed. Thus, there is a one-to-one correspondence of the relative momentum between the two nucleons to the energy of the proton detected at 30° ($E1$). The cross section $\sigma_{\rm seq}$ can then be calculated point by point along the kinematic locus, and projections of the result can be made on either axis. A numerical integration was performed over the target and both detectors' areas.

Individual projections due to ρ_{13}, ρ_{12}, and ρ_{23} were calculated and a least-squares fit to the data was made

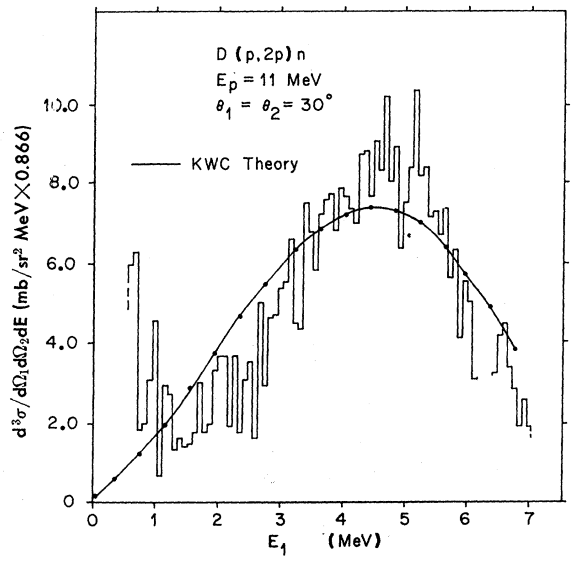

FIG. 12. Fits to the $E_p=11$ MeV, $\theta_1=30°$, $\theta_2=30°$ data with the KWC form of the spectator-model calculation. Neither the detector energy resolution nor energy losses in the target are folded in.

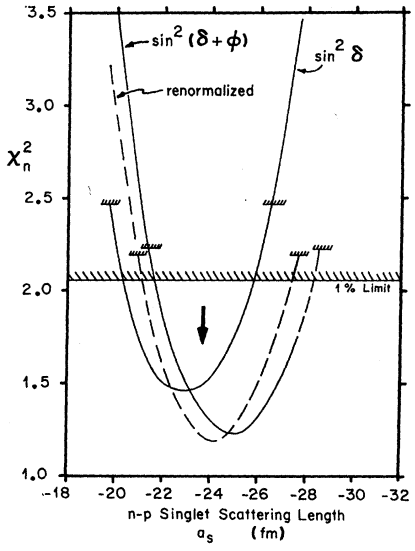

FIG. 14. χ_n^2 versus a_{np} curves for the $E_p=11$ MeV, $\theta_1=30°$, $\theta_2=77°$ data with the three forms of DOS functions given by Eqs. (2), (3), and (4). The renormalized form gives a value of $a_{np}=-24.2$ fm, which is closest to the accepted value of −23.7 fm, which is indicated by the arrow. The C's and other parameters are the same as in Fig. 13.

in order to determine the weighting factors C_{13}, C_{12}, and C_{23}. Before the least-squares fit was made, the detector energy resolution function and the energy loss in the target were folded into the individual DOS. Typical values of the weighting factors for the energy range 9–13 MeV were $C_{13}=C_{23}=1$, $C_{12}=0.3$. Using these calculated values of the weighting factors, it was found that

$$C_{12}\rho_{12}+C_{23}\rho_{23}\simeq 0.05C_{13}\rho_{13} \qquad (9)$$

for the region of the peak where $E_{13}{}^{+}\leq 300$ keV.

Fits to the $E_p=11$ MeV, $\theta_1=30°$, $\theta_2=77°$ data with the three forms of the DOS are shown in Fig. 11. In this case, $C_{13}=C_{12}=C_{23}=1$, $a_{np}=-23.71$ fm, $r_{0\,np}=2.5$ fm, $a_{pp}=-7.69$ fm, $r_{0\,pp}=2.81$ fm and no target energy losses were taken into account. The best fit for the spectrum was obtained by the renormalized form so that this form was used in all calculations thereafter.

2. Quasifree knockout. The KWC[14] form of the spectator-model calculation was used to fit the spectra at those angles where the spectator neutron energy dropped below 1 MeV while the relative energies between pairs of nucleons stayed above 300 keV. The expression for the cross section is

$$d\sigma/d\Omega_1 d\Omega_2 dE_1=(d\sigma/d\Omega)_f\,|\,\phi(p_3)\,|^2\mathfrak{I}, \qquad (10)$$

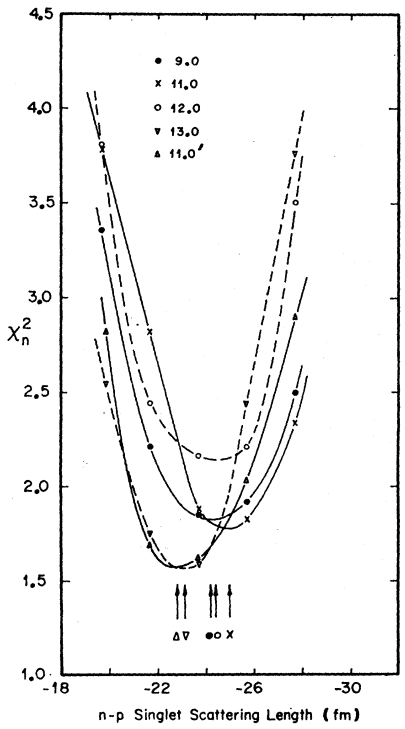

FIG. 15. $\chi_n{}^2$ versus a_{np} curves for the five statistically most significant spectra. The values of C_{13}, C_{12}, and C_{23} were determined by a least-squares fit to the total spectra in each case. The detector resolution function and energy losses in the target were folded in. Table III gives the a_{np} obtained from the individual curves. The arrows indicate these values of a_{np}.

TABLE III. Results of χ^2 analysis for a_{np}.

E_p (MeV)	θ_1-θ_p (deg)	a_{np} (at min χ^2) (fm)
9.0	30-73.7	−24.2
11.0	30-77.4	−25.0
11.0	30-77	−22.8
12.0	30-78.7	−24.4
13.0	30-79.9	−23.1
Average $a_{np}=-23.9\pm0.8$ fm		

where $d\sigma/d\Omega$ is the free proton-proton cross section, $\mathfrak{I}$ is a phase-space factor, and $\phi(p_3)$ is the Fourier transform of the initial deuteron bound-state wave function with p_3 being the momentum transferred to the spectator neutron. Using the Hulthen wave function for the deuteron,

$$\phi(p_3)=[8\pi\alpha\beta(\alpha+\beta)^3]^{1/2}[(\alpha^2+p_3{}^2/\hbar^2)(\beta^2+p_3{}^2/\hbar^2)]^{-1}, \qquad (11)$$

where $\alpha=0.232\times10^{13}$ cm^{-1} and $\beta=1.202\times10^{-13}$ cm^{-1}. Unfortunately, neither the impulse approximation nor the requirement that the bombarding energy be much larger than the binding energy of the deuteron is valid at the energies used in this experiment. Still, a rather good qualitative fit to the data was obtained as can be seen from Fig. 12. The calulated curve has a greater width than the data and gives a higher cross section by an order of magnitude. However, the position of the peak is quite well reproduced.

Other data at higher energies[3,13,14] are fitted progressively better with increasing energy, although even at $E_p=145$ MeV, the calculated curve is broader than the experimental peak and predicts a higher cross section.

B. *n-p* Singlet Scattering Length

Analyzing the 11 MeV, $\theta_1=30°$, $\theta_2=77°$ data using the values of scattering length and effective range determined from elastic scattering experiments,[26] it was found that the renormalized form of the DOS gave the best fit (see Fig. 11). All of the χ^2 fits are made to that region of the spectrum where the *n-p* relative energy falls below 300 keV. Figure 13 shows the best fits to the same data using the renormalized DOS and varying the a_{np}. It is apparent that the $a_{np}=-23.71$ fm curve agrees with the data better than the −19.71 or −27.71 fm curves. A χ^2 analysis gives a minimum in the χ^2 for the renormalized DOS at −24.2 fm, at −22.9 fm for the Watson form, and at −25.1 fm for the $\sin^2(\delta+\phi)$

[26] H. P. Noyes, Phys. Rev. **130**, 2025 (1963); M. A. Preston, *Physics of the Nucleus* (Addison-Wesley Publishing Company, Inc., Reading, Mass., 1962).

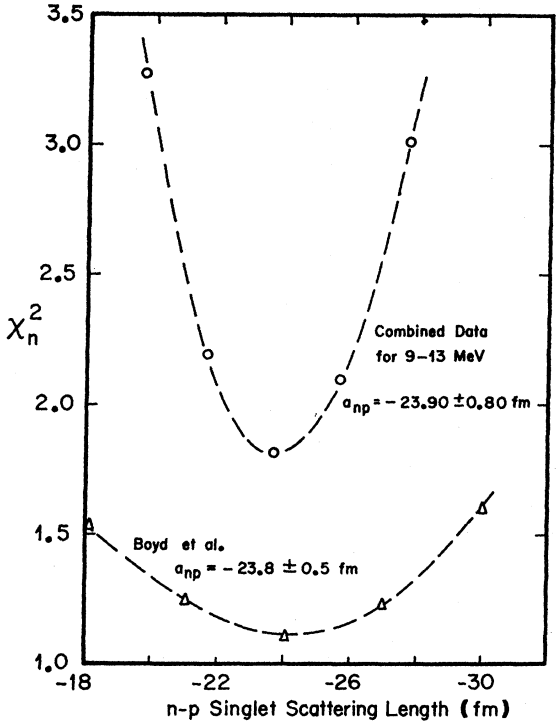

FIG. 16. The combined χ_n^2 curve for the five spectra listed in Table III. An example of the χ^2 curves of Boyd and Donovan from which $a_{np}=-23.8\pm0.5$ fm was obtained is also shown. The mean value of these five equally weighted, independently measured values of a_{np} is -23.9 ± 0.8 fm, where the quoted error is 1 standard deviation.

form (see Fig. 14). In this case and all subsequent cases, the χ^2 was calculated for $a_{np}=-19.71$, -21.71, -23.71, -25.71, and -27.71 fm while keeping $r_{0\,p\text{-}n}=2.5$ fm, $a_{pp}=-7.69$ fm, and $r_{0\,pp}=2.81$ fm. No search on $r_{0\,p\text{-}n}$ was made owing to a lack of available computer time. C_{13}, C_{12}, and C_{23} were all set to 1 in the above analysis and energy losses in the target were not folded in.

A more careful analysis was performed on the spectra listed in Table III with the minimum positions in the χ^2 curves also shown. These individual χ^2 curves are shown in Fig. 15. This analysis differed from the earlier one in two aspects. (1) C_{13}, C_{12}, and C_{23} were the values determined by a least-squares fit to the total spectrum in each case. (2) The energy loss in the target was folded into the calculated spectra. Since the polyethylene targets deteriorate quite quickly under beam bombardment, the spot on the target struck by the beam was changed every 1–2 h. The change in the total target thickness was estimated to be less than 10%. In all cases, the absolute energy scale was assumed uncertain to ±160 keV and the data were shifted in 16-keV steps until the minimum in the χ^2 was found. In general, less than 32 keV of shift was needed to obtain the minimum χ^2. Only those channels in which the $E_{13}{}^{+}\lesssim300$ keV were incorporated into the χ^2 analysis.

Figure 16 shows the combined χ^2 curve for all five spectra. One of the χ^2 curves of Boyd and Donovan from which an n-p scattering length of -23.8 ± 0.5 fm was obtained is also shown.

The mean value of the five equally weighted, independently measured values of a_{np} (see Table III) is -23.9 ± 0.8 fm, where the quoted error is one standard deviation. Although this value of a_{np} is not as accurate as the one obtained from elastic scattering experiments, it is one of the best values of the nucleon-nucleon scattering lengths obtained from reactions with three particles in the final state. Since this type of reaction is the only one from which a_{nn} can be extracted, there is now hope that a more accurate value of a_{nn} can be obtained, provided that the other obscuring effects discussed above are carefully minimized.

One further point that must be made is that there was a relatively small change in the value of the scattering length with the change in one kinematic variable, namely, E_p. In kinematically incomplete experiments, the experience has been that by varying the bombarding energy or the angle at which one of the three final-state particles is detected, a considerable change occurs in the extracted scattering length.

ACKNOWLEDGMENTS

The authors wish to thank Dr. S. T. Emerson, Dr. M. C. Taylor, Dr. R. J. Spiger, and J. Sandler for valuable assistance in all stages of the experiment. For many useful discussions, we are thankful to Dr. T. Canada. We wish to thank Dr. W. D. Simpson for the use of his DOS analysis programs. Many of the problems associated with the preliminary analysis programs were ably handled by Hugh Jones and Miss Sandra Harrison. For his untiring efforts at debugging the new IBM-1800 computer-analyzer interfacing hardware, thanks are due J. Buchanan.

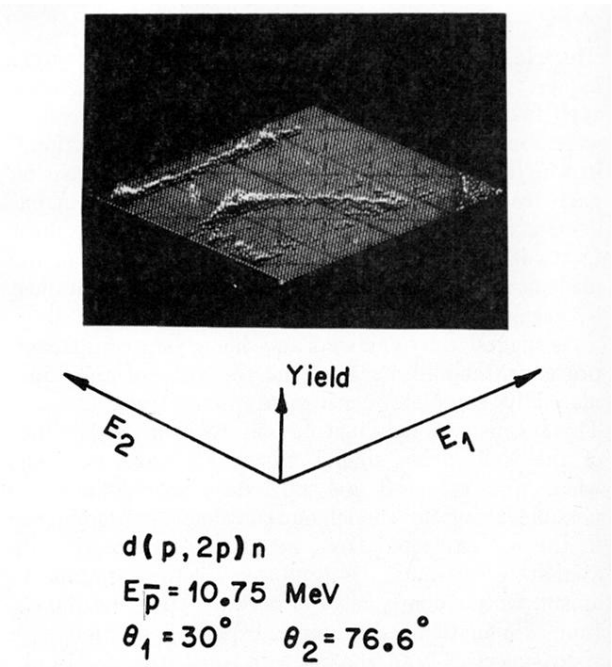

FIG. 3. Photograph of the computer oscilloscope display for a typical run. Population along the curved band is due to the $d(p, 2p)n$ reaction. The straight lines are due to accidental from p-d elastic and p-^{12}C inelastic processes.